Journal of the Association of Arab Universities for Basic and Applied Sciences (2017) 22, 45–54

University of Bahrain

Journal of the Association of Arab Universities for Basic and Applied Sciences

www.elsevier.com/locate/jaaubas
www.sciencedirect.com

ORIGINAL ARTICLE

Chromenopyridin derivatives as environmentally benign corrosion inhibitors for N80 steel in 15% HCl

K.R. Ansari [a], M.A. Quraishi [a,*], Ambrish Singh [b]

[a] Department of Chemistry, Indian Institute of Technology, Banaras Hindu University, Varanasi 221005, India
[b] Department of Chemistry, Lovely Faculty of Technology and Sciences, Lovely Professional University, Phagwara, India

Received 24 June 2015; revised 3 November 2015; accepted 5 November 2015
Available online 10 December 2015

KEYWORDS

N80 steel;
HCl;
SEM;
Corrosion

Abstract This research work was to investigate the corrosion inhibition performance of two newly synthesized chromenopyridine derivatives namely 2,4-diamino-5-(phenylthio)-5H-chromeno[2,3-b] pyridine-3-carbonitrile (PPC-1) and 2,4-diamino-5-phenoxy-5H-chromeno[2,3-b]pyridine-3-carboni trile (PPC-2) as potential environmentally friendly corrosion inhibitors for N80 steel in 15% hydrochloric acid (HCl). Various techniques like gravimetric, electrochemical impedance spectroscopy (EIS), Tafel polarizations, scanning electron microscope (SEM) and atomic force microscopy (AFM) have been used. The inhibition efficiencies given by PPC-1 and PPC-2 at 200 mg L^{-1} are 92.4% and 82.1% respectively. Tafel polarization revealed that both inhibitors are cathodic in nature. Langmuir adsorption isotherm was found to be the best fit. The experimental result was further supported by quantum chemical study.

1. Introduction

In the petroleum industry oil extraction equipment is generally made from N80 steel. Usually 15% hydrochloric acid (HCl) is pumped in order to etch rocks, which are incorporated into the conductive channels of the wellbore. This process improves the permeability of the oil reservoir, which in turn increases the recovery efficiency of oil. In the absence of a corrosion inhibitor, there would be damage of the oil extraction equipment and the crude oil would pollute the soil. So, addition of corrosion inhibitors is an effective way to reduce corrosion. Commonly used corrosion inhibitors in acidic media are heterocyclic compounds, with π-electrons, aromatic rings and heteroatoms such as sulfur, nitrogen and oxygen in their structure (Ansari et al., 2012, 2014; Ansari and Quraishi, 2015a; Mohamed and Rehim, 2015; Karthikaiselvi and Subhashini, 2014).

However, in the view of the strong environmental regulations, research has to focus in the field of corrosion to develop those inhibitors which are environmentally benign. In order to move on the said statement we have synthesized the chromenopyridine derivatives, which are acting as anti proliferative, cancer chemo preventive, antibacterial, antimyopic, antihistaminic, hypertensive, antirheumatic and antiasthmatic activities (Evdokimov et al., 2007).

* Corresponding author. Tel.: +91 9307025126; fax: +91 542 2368428.
E-mail addresses: maquraishi@rediffmail.com, maquraishi.apc@itbhu.ac.in (M.A. Quraishi).
Peer review under responsibility of University of Bahrain.

http://dx.doi.org/10.1016/j.jaubas.2015.11.003
1815-3852

Quantum chemical calculations have extensively been used for correlating the molecular structure of inhibitors and their inhibition properties (Musa et al., 2011; Xia et al., 2008).

The present study was focused on the use of two chromenopyridine derivatives namely 2,4-diamino-5-(phenyl thio)-5H-chromeno[2,3-b]pyridine-3-carbonitrile (PPC-1) and 2,4-diamino-5-phenoxy-5H-chromeno[2,3-b]pyridine-3-carbo nitrile (PPC-2) as a corrosion inhibitor for N80 steel in 15% HCl using gravimetric measurements, polarization measurements, electrochemical impedance spectroscopy, scanning electron microscopy (SEM), atomic force microscopy (AFM) and quantum chemical calculations.

2. Experimental details

2.1. Synthesis of inhibitor (PPC's)

The synthesis of inhibitors was carried in the laboratory according to the following procedure (Evdokimov et al., 2007). Salicylaldehyde (1.5 mmol), malononitrile (3 mmol) and thiol/phenol (1.5 mmol) in 7 mL of ethanol were taken in a round bottom flask. To this solution Et_3N (0.1 mmol) was added dropwise at room temperature. The resulting mixture was refluxed for 3–3.5 h and then allowed to cool to room temperature. The precipitate formed was filtered and the product was dissolved in 3 mL DMF and the remaining undissolved material was removed by filtration. To the filtrate 4 mL water was added, which resulted in the crystallization of the product. The formed crystals were isolated by filtration to yield a corresponding pure chromenopyridine.

The synthetic scheme and molecular structure of the inhibitors are given in Fig. 1(a–c).

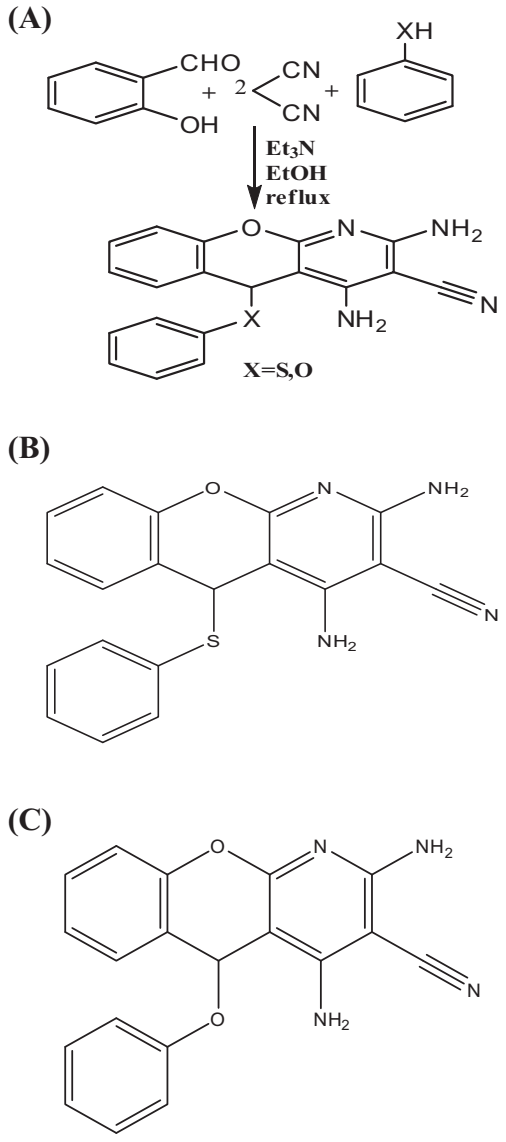

Figure 1 (a) Synthetic route of PPCs. (b and c) Molecular structure of PPCs (a) PPC-1, (b) PPC-2.

2.2. Gravimetric experiments

N80 steel used for the corrosion test has the following composition (wt%): C 0.31; Si 0.19; Mn 0.92; P 0.010; S 0.008; Cr 0.2, balance iron. The dimensions of the N80 steel used for gravimetric and electrochemical experiments are 5.0 cm × 2.5 cm × 0.2 cm and 2.0 cm × 1.0 cm × 0.025 cm. All corrosion tests were performed in 15% HCl for a 6 h immersion. The corrosion rate C_R (mg cm^{-2} h^{-1}) was calculated by using the following equation:

$$C_R = \frac{W}{At} \tag{1}$$

where W is the average weight loss of a N80 steel strip, A the total area of a N80 steel strip and t is immersion time (6 h).

The inhibition efficiency (η%) was estimated by using the following equation (Ansari et al., 2015):

$$\eta\% = \frac{C_R - C_{R(i)}}{C_R} \times 100. \tag{2}$$

Surface coverage (θ) was calculated using the following relationship (Ansari et al., 2015)

$$\theta = \frac{C_R - C_{R(i)}}{C_R}. \tag{3}$$

2.3. Electrochemical measurement

Electrochemical experiments were carried out using a three-electrode cell assembly where the N80 steel strip with an exposed area of 1 cm^2 was used as a working electrode, graphite rod as a counter electrode and saturated calomel electrode (SCE) as a reference electrode. The working electrode was immersed in the test solution at open circuit potential (OCP) for 30 min before measurement in order to attain a steady state condition. For all electrochemical measurements, GamryPotentiostat/Galvano stat (Model G-300) connected with a personal computer with EIS software Gamry Instruments Inc., USA. The analyses of experiments were carried out using Echem Analyst 5.0 software package.

The potentiodynamic polarization measurements were performed by changing the electrode potential automatically from −250 to +250 mV versus SCE at OCP at a scan rate of 1 mV s^{-1}.

Impedance measurements were carried out by an AC signal with the amplitude of 10 mV peak to peak at the open circuit potential in the range of 100 kHz to 0.01 Hz frequency. All

electrochemical measurements i.e. potentiodynamic polarization and impedance were carried out at 308 K.

2.4. Surface analysis: SEM and AFM

In order to get insights into the changes on the surface of corrosive samples before and after the addition of inhibitors, the specimens were first immersed in 15% HCl in the absence and presence of optimum concentration (200 mg L^{-1}) of ADP and AMP for 6 h at 308 K, respectively, taken out from the test solutions, cleaned with bi-distilled water and dried. SEM images were conducted using a Ziess Evo 50 XVP instrument model, at an accelerating voltage of 5 kV and a magnification 5k×. The instrument used for AFM is (AFM, NT-MDT SOLVER Next AFM/STM). The scan size of each sample is 10 μm × 10 μm.

2.5. Quantum chemical calculations

Gaussian 03-program package was used for all Quantum chemical calculations (Frisch, 2007). DFT (B3LYP) optimized the molecular structures of inhibitors, in combination with the 6-31G(d, p) basis set. The following quantum chemical indices were taken into consideration: energy of the highest occupied molecular orbital (E_{HOMO}), energy of the lowest unoccupied molecular orbital (E_{LUMO}) and energy gap: $\Delta E = E_{LUMO} - E_{HOMO}$. All calculations were carried out both on neutral and protonated molecules.

3. Results and discussion

3.1. Electrochemical measurements

3.1.1. Electrochemical impedance spectroscopy

Electrochemical impedance spectroscopy (EIS) was used to investigate the surface layer created by the adsorbed PPC molecules. The impedance behavior of the PPC molecules in the concentration range of 50–200 mg L^{-1} on N80 steel in 15% HCl at 308 K is shown in Fig. 2(a and b). The inspection of the Nyquist plots for PPC-1 and PPC-2 with increasing concentrations of the PPCs are almost showing a similar trend i.e. increase in semicircle diameter with an increase in concentration. By applying the equivalent circuit (Fig. 2(c)) the following impedance parameters were extracted, such as solution resistance (R_s), the charge transfer resistance (R_{ct}) and the constant phase element (CPE) and are listed in Table 1. Fitness accuracy of this circuit was checked by plotting the simulated Nyquist plots of PPCs and are shown in Fig. 2(d and e) The impedance of the CPE can be given as follows (Ansari and Quraishi, 2015b)

$$Z_{CPE} = Y_0^{-1}(j\omega)^{-n} \tag{4}$$

where Y_0 is the amplitude comparable to a capacitance, j is the square root of −1, ω is angular frequency and n is the phase shift.

Double layer capacitance (C_{dl}) can be calculated as follows

$$C_{dl} = \frac{Y\omega^{n-1}}{\sin(n(\pi/2))} \tag{5}$$

where, ω is the angular frequency ($\omega = 2\pi f_{max}$) at which the imaginary part of impedance ($-Z_{im}$) is maximal and n is the phase shift.

The data in Table 1 reveal that the increase in the values of charge transfer resistance is associated with a decrease in the double-layer capacitance. This is because as the PPCs molecules are adsorbed on the N80 steel surface, replacement of water molecules takes place, which in turn causes the decrease in the C_{dl} values and an increase in R_{ct} values. Also inhibition efficiency of the inhibitor can be calculated by using charge transfer resistance according to the following equation (Solomon et al., 2010)

$$\eta\% = \left(1 - \frac{R_{ct}}{R_{ct(i)}}\right) \times 100 \tag{6}$$

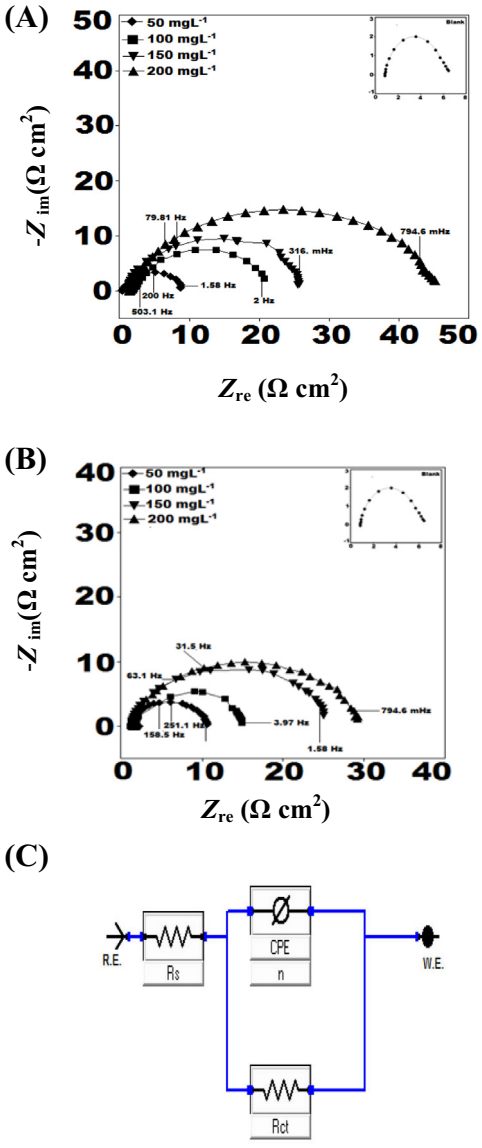

Figure 2 (a and b) Nyquist plots for mild steel in 15% HCl, in the absence and presence of different concentrations of PPCs at 308 K for (a) PPC-1, (b) PPC-2, (c) Equivalent circuit models used to fit the EIS data, (d and e) Fitted Nyquist plots (d) PPC-1, (e) PPC-2.

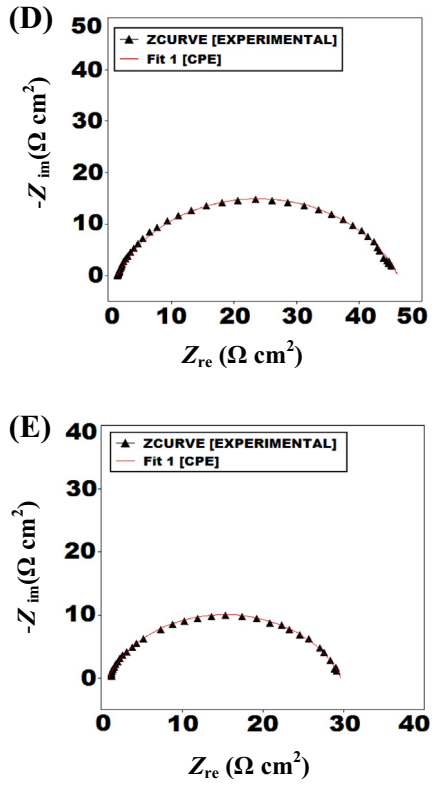

Fig. 2 (*continued*)

R_{ct} and $R_{ct(i)}$ respectively represent the charge transfer resistance in absence and presence of inhibitors. Table 1, reveals that as the concentration of the inhibitor is increased, inhibition efficiency is increased.

3.1.2. Tafel polarization

The Tafel polarization curves of N80 steel at different concentrations of PPCs are shown in Fig. 3(a and b) at 308 K. Different electrochemical parameters i.e. corrosion potential (E_{corr}), corrosion current density (I_{corr}), anodic Tafel slopes (β_a), cathodic Tafel slopes (β_c) and inhibition efficiency ($\eta\%$) are reproduced in Table 2. Inhibition efficiency ($\eta\%$) was calculated by using the following equation:

$$\eta\% = \left(1 - \frac{I_{corr(i)}}{I_{corr}}\right) \times 100 \quad (7)$$

where I_{corr} and $I_{corr(i)}$ are the uninhibited and inhibited corrosion current densities, respectively.

The observation of Table 2 proves that the value of I_{corr} is going to decrease as the PPC concentration increased from 50 to 200 mg L^{-1}, which indicates the retardation of the corrosion process (Obot et al., 2010). Also a slight change occurs in β_a and β_c values with increasing the concentration of the PPCs i.e. their values are almost constant. This explains that PPC molecules are adsorbed over the N80 steel surface and slow down the corrosion process by just blocking the reaction sites which are present over the N80 steel surface without changing the mechanism of metal dissolution (Ahamad et al., 2010; Negm et al., 2011). From Fig. 3(a and b) it is revealed that PPCs notably accelerate the anodic reaction at all concentrations, and only inhibited the cathodic reaction. In general, classification of the inhibitor as anodic or cathodic is based on the displacement of E_{corr} values of the inhibitor with respect to the blank i.e. if the displacement is more than 85 mV, the inhibitor is said to be anodic or cathodic (Ferreira et al., 2004). In the present study both PPC-1 and PPC-2, E_{corr} value shift toward a more negative direction and the maximum shift is 245 mV in PPC-1 and 227 mV in PPC-2 with respect to the blank. Thus the overall discussion reveals that both the PPCs are cathodic inhibitors.

3.2. Effect of inhibitor concentration

The effect of inhibitor concentration on inhibition efficiencies in the range of 50 to 200 mg L^{-1} are given in Fig. 4(a) and are obtained by gravimetric study. The inspection of Fig. 4 (a) reveals that inhibition efficiency increases with an increase in PPCs concentration.

3.3. Effect of temperature

As the temperature increases, the inhibition efficiency in both PPC-1 and PPC-2 decreases, and it is shown in Fig. 4(b). This reveals that an increase in temperature diminished the protective effect of the PPCs.

The Arrhenius plots are used for the calculation of activation energy (E_a), which is a plot, between corrosion rate

Table 1 Electrochemical impedance parameters for N80 Steel in 15% M HCl in the absence and presence of different concentrations of PPCs at 308 K.

Inhibitor	C_{inh} (mg L^{-1})	R_s (Ω cm^2)	R_{ct} (Ω cm^2)	n	Y_0 (μF/cm^2)	C_{dl} (μF/cm^2)	η (%)
Blank	–	0.820	4.58	0.755	603	134.24	–
PPC-1	50	0.331	8.66	0.782	375	105.66	47.1
	100	1.943	18.05	0.827	252	96.11	74.6
	150	1.244	23.53	0.898	85	53.88	80.5
	200	1.390	42.61	0.927	42	29.71	89.2
PPC-2	50	1.631	7.25	0.771	484	118.28	36.8
	100	1.939	11.17	0.802	290	99.65	59.0
	150	1.605	16.39	0.858	116	56.54	72.06
	200	1.407	26.81	0.892	60	35.26	82.91

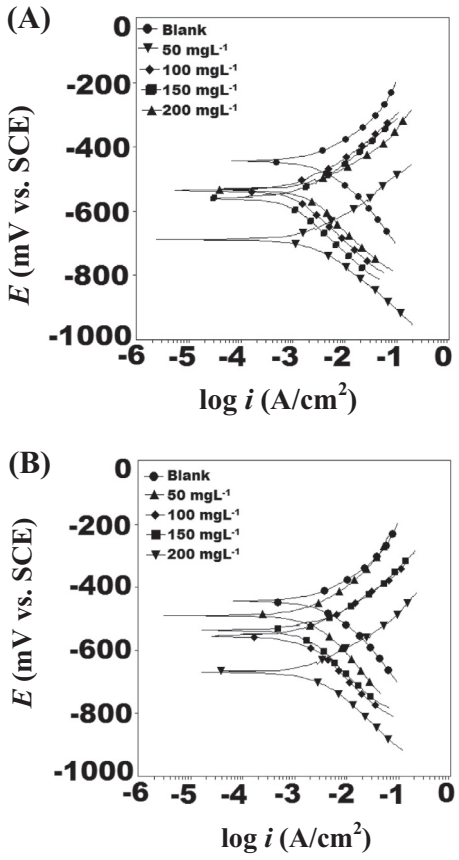

Figure 3 (a and b) Tafel curves for N80 steel in 15% HCl in the absence and presence of different concentrations of inhibitors at 308 K for (a) PPC-1, (b) PPC-2.

[C_R (mg cm^{-2} h^{-1})] vs. T and can be given by the following relation:

$$C_R = A \exp\left(\frac{-E_a}{RT}\right) \tag{8}$$

where E_a is the activation energy, T is the absolute temperature, A is the Arrhenius pre-exponential constant and R is the universal gas constant. The Arrhenius plots are represented by Fig. 4(c). The values of E_a are calculated from the slope of the plots (Fig. 4(c)). In the absence of inhibitor the value of E_a is 34.58 kJ mol^{-1} and as the inhibitors are added it becomes 60.54 kJ mol^{-1} (PPC-1) and 50.55 kJ mol^{-1} (PPC-2) respectively at their optimum concentration (200 mg L^{-1}). The above E_a values in the presence of PPCs are larger than in their absence, but lower than 80 kJ mol^{-1}, which is the threshold value for chemical adsorption. This suggests physical adsorption of PPC molecules.

Arrhenius equation can also be written as follows:

$$C_R = \frac{RT}{Nh} \exp\left(\frac{\Delta S^*}{R}\right) \exp\left(-\frac{H^*}{RT}\right) \tag{9}$$

A straight line is obtained by plotting a graph between log C_R/T vs. $1/T$ (Fig. 4(d)). By using the slope and intercept values, ΔH^* and ΔS^* can be calculated. The values of ΔH^* and ΔS^* in the absence of PPCs are 31.90 kJ mol^{-1} and -101.24 J K^{-1} mol^{-1} respectively. The values of $\Delta H^*$and ΔS^* for PPC-1 are 58.11 kJ mol^{-1} and -36.36 J K^{-1} mol^{-1}, and for PPC-2 are 48.06 kJ mol^{-1} and -62.94 J K^{-1} mol^{-1}. ΔH^* values in the presence of PPCs are higher than in their absence, which indicates the slower dissolution of N80 steel (Guan et al., 2004). The values of ΔS^* is more in the presence of PPCs as compared to the blank. This is because as the PPC molecules are adsorbed over the N80 steel surface, it causes the displacement of the pre-adsorbed water molecules, which increases the randomness of the system (Dahmani et al., 2010). So, this causes the increase in entropy, which is basically an increase in solvent (water) entropy.

3.4. Adsorption isotherm

Adsorption isotherm was used in view of gathering information on the interaction of PPCs molecules and N80 steel surface. By fitting different isotherms like Langmuir, Temkin, Frumkin and Langmuir. Only Langmuir adsorption isotherm, which is plot between C/θ against C, provides the best fit with regression coefficient (R^2) approaching toward 1. Langmuir adsorption isotherm can be given by the following equation (Bammou et al., 2014; Anejjar et al., 2014):

$$C/\theta = 1/K_{ads} + C \tag{10}$$

where θ is the surface coverage, C is the inhibitor concentration, K_{ads} is the equilibrium constant of adsorption process. The Langmuir adsorption isotherms of PPCs are shown in Fig. 4(e).

Table 2 Electrochemical polarization parameters for N80 Steel in 15% M HCl in the absence and presence of different concentrations of PPCs at 308 K.

Inhibitor	C_{inh} (mg L^{-1})	E_{corr} (mV/SCE)	I_{corr} (μA/cm^2)	β_a (mV/dec)	$-\beta_c$ (mV/dec)	η (%)
Blank	–	−443	3201	85.7	100.8	–
PPC-1	50	−688	1701	103.2	107.1	46.8
	100	−533	837	65.6	92.6	73.8
	150	−561	702	86.9	108.9	78.0
	200	−536	241	66.9	74.2	92.4
PPC-2	50	−489	1890	82.3	97.8	40.9
	100	−536	1400	79.6	96.3	56.2
	150	−527	998	99.6	108.5	68.8
	200	−670	572	69.6	91.4	82.1

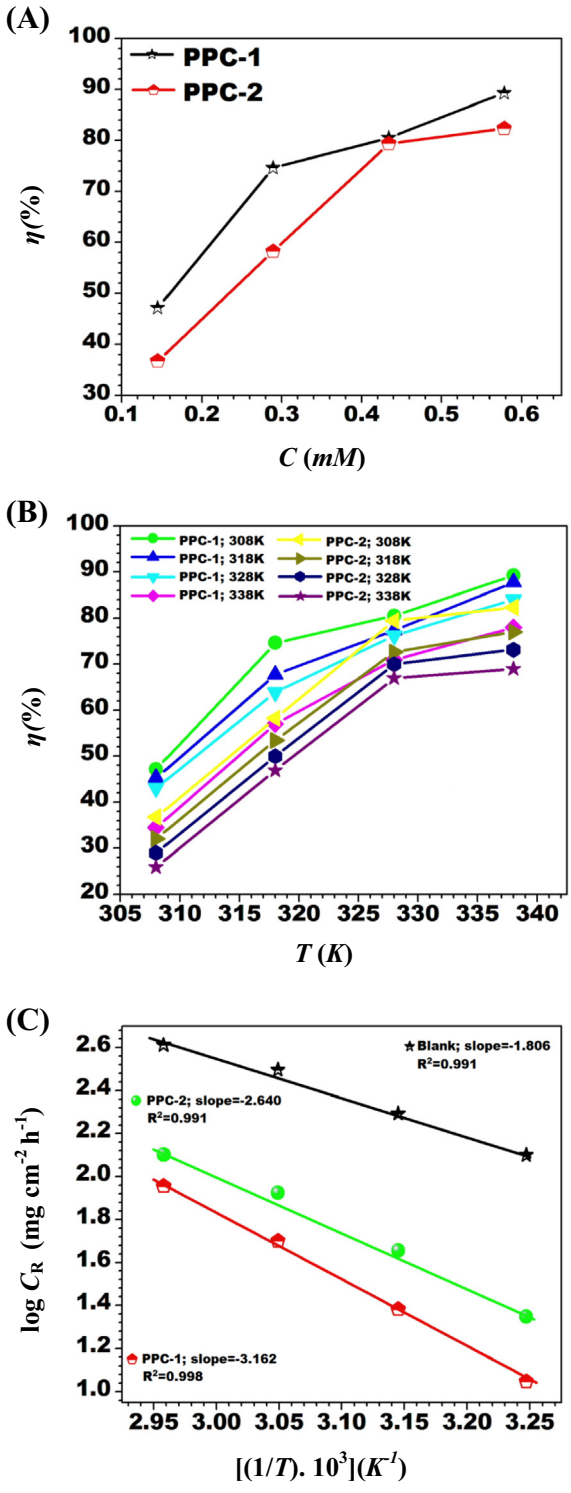

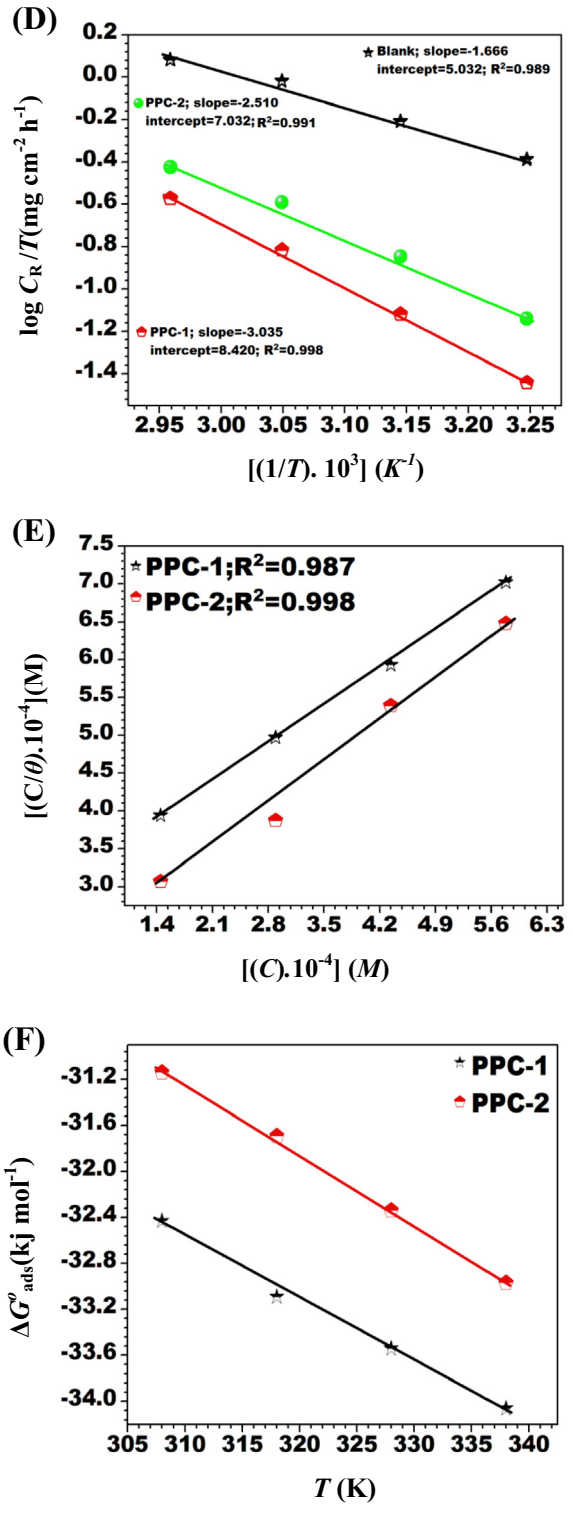

Figure 4 (a) Variation of inhibition efficiency ($\eta\%$) with inhibitor concentration at 308 K. (b) Variation of inhibition efficiency ($\eta\%$) with temperature. (c) Arrhenius plot of N80 steel in 15% HCl in the absence and presence of optimum concentration of PPCs. (d) Transition-state plot of N80 steel in 15% HCl in the absence and presence of optimum concentration of PPCs. (e) Langmuir's isotherm plots for adsorption of inhibitors on N80 steel surface in 15% HCl. (f) ΔG°_{ads} versus T plot for N80 steel in 15% HCl solution with different concentrations of PPCs.

Fig. 4 (*continued*)

The equilibrium constants (K_{ads}) and standard free energy of adsorption (ΔG°_{ads}) are correlated according to the equation (Verma et al., 2016):

$$\Delta G^{\circ}_{ads} = -RT\ln(55.5\,K_{ads}) \quad (11)$$

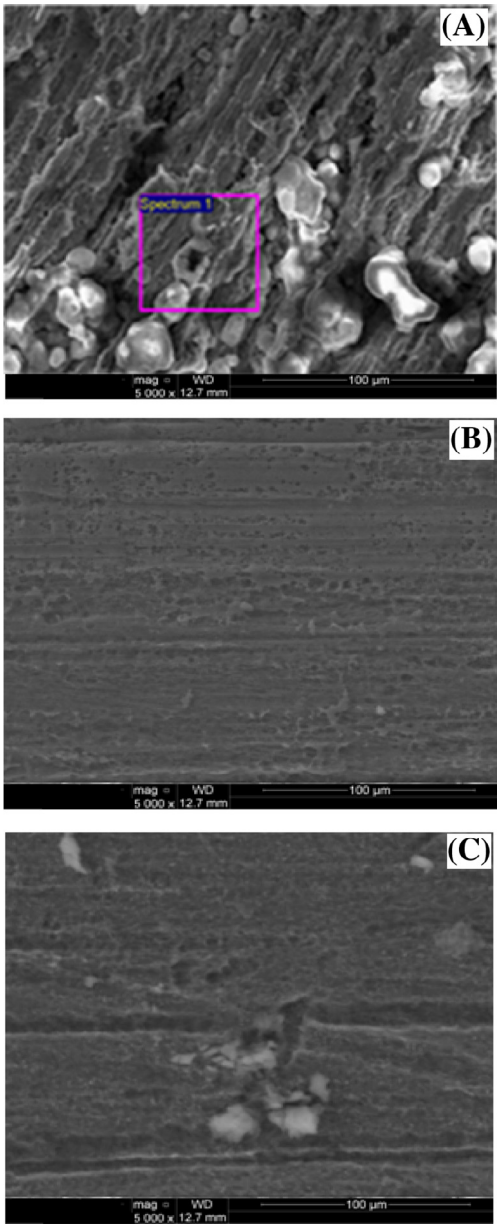

Figure 5 (a–c) SEM micrographs of N80 steel surfaces (a) blank 15% HCl, (b) PPC-1, (c) PPC-2.

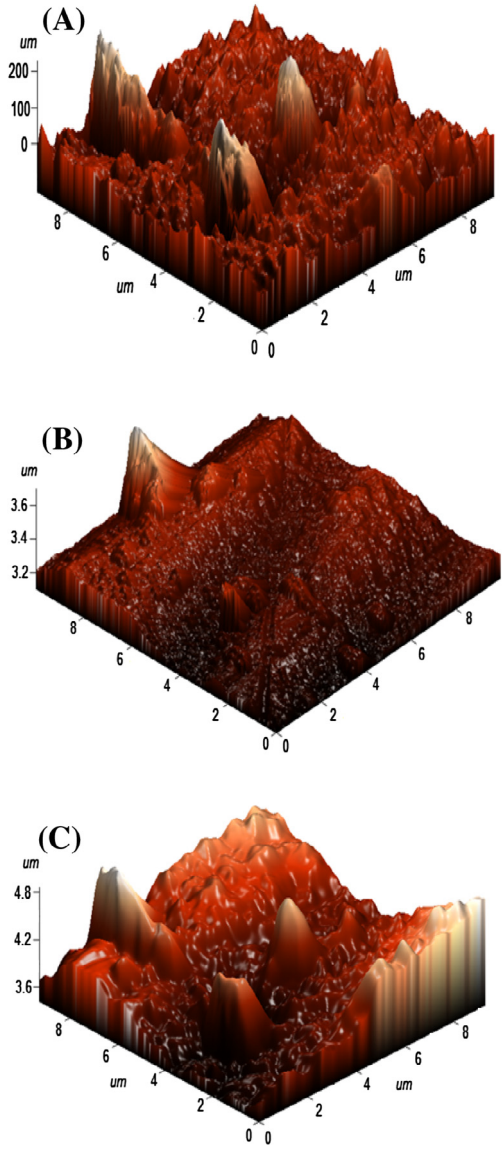

Figure 6 (a–c) AFM images (a) inhibited, (b) PPC-1, (c) PPC-2.

where R is the gas constant and T is the absolute temperature. 55.5 is the concentration of water in solution in mol L^{-1}.

K_{ads} values are calculated from the intercepts of the straight lines and are as follows 5.68×10^3 M^{-1} (PPC-1) and 3.42×10^3 M^{-1} (PPC-2).

In the present study ΔG_{ads} adsorption values are 32.42 kJ mol^{-1} (PPC-1) and 31.13 kJ mol^{-1}, which is less than the threshold value (−40 kJ mol^{-1}), showing that PPCs adsorption is physical.

The thermodynamic parameters, enthalpy of adsorption (ΔH°_{ads} kJ mol^{-1}) can be calculated from the rearranged Gibbs–Helmholtz Eq. (12).

$$\Delta G^{\circ}_{ads} = \Delta H^{\circ}_{ads} - T\Delta S^{\circ}_{ads} \quad (12)$$

Fig. 4(f) shows the dependence of ΔG°_{ads} on T, which indicates an appropriate relationship between thermodynamic parameters. The negative sign of ΔH°_{ads} shows that the adsorption process is exothermic (Shukla and Ebenso, 2011).The numeric values of ΔH°_{ads} are −16.01 kJ mol^{-1} (PPC-1) and −12.20 kJ mol^{-1} (PPC-2) which shows that these molecules involve the physical adsorption mechanism (Rosenfeld, 1981).

3.5. Surface analysis: SEM and AFM

The morphology of N80 steel surfaces was explored by using SEM micrographs, and are shown in Fig 5a–c. Observation of Fig. 5a showed a rough, damaged and extremely corroded surface in the absence of PPCs. Fig. 5(b and c), are the micrographs in PPC-1 and PPC-2 respectively, here the morphology is nearly smooth. This revealed that PPCs have been adsorbed over the N80 steel surface and reduce the corrosion process.

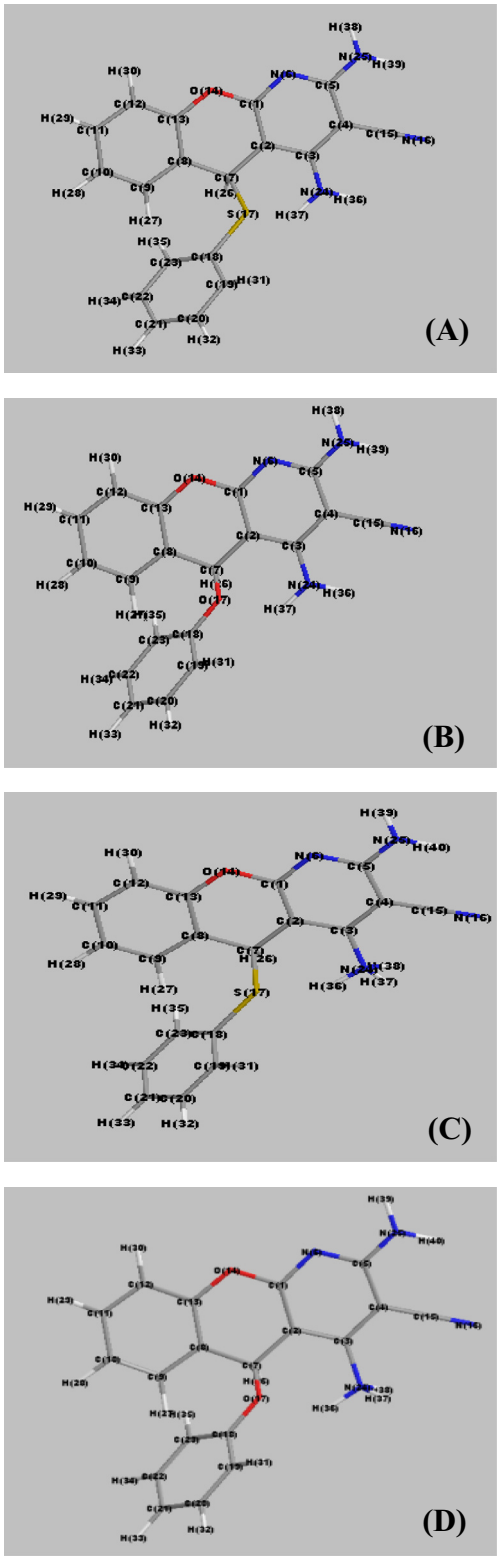

Figure 7 (a–d) Optimized structures of inhibitor (a) neutral PPC-1, (b) neutral PPC-2, (c) protonated PPC-1, (d) protonated PPC-2.

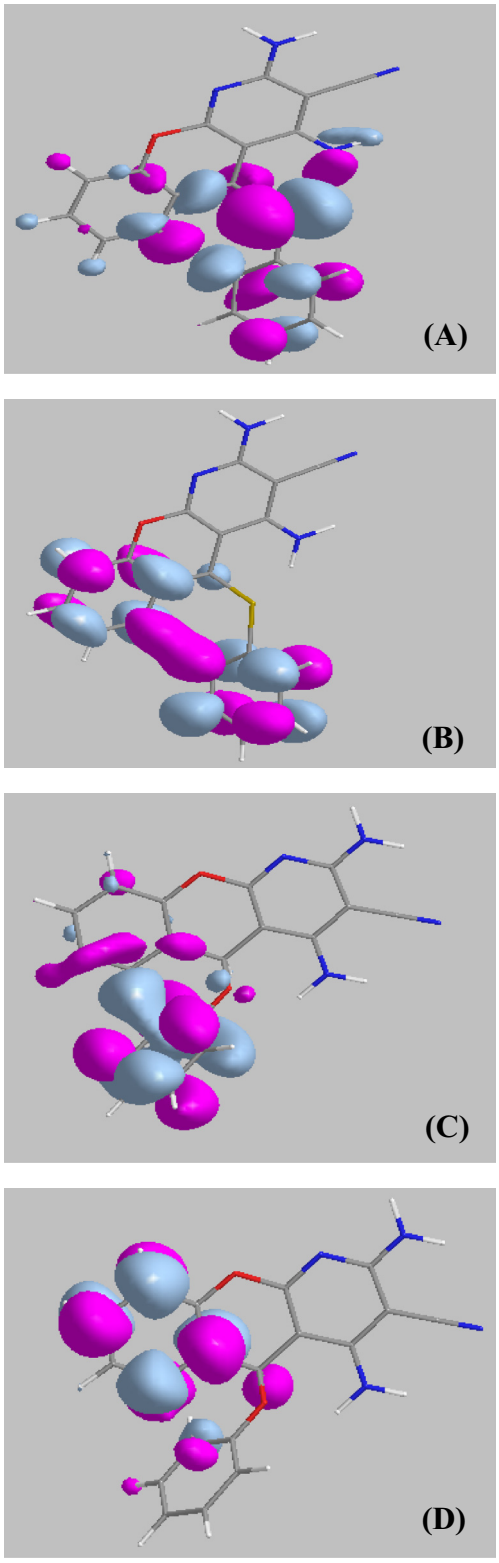

Figure 8 (a–d) Frontier molecular orbital's of neutral PPC-1 (a) HOMO, (b) LUMO and PPC-2 (c) HOMO, (d) LUMO.

The three dimensional (3D) AFM morphologies in the absence and presence of PPCs are shown in Fig 6(a–c). The parameters calculated are R_q (Root-mean-square roughness) and R_a (average roughness).

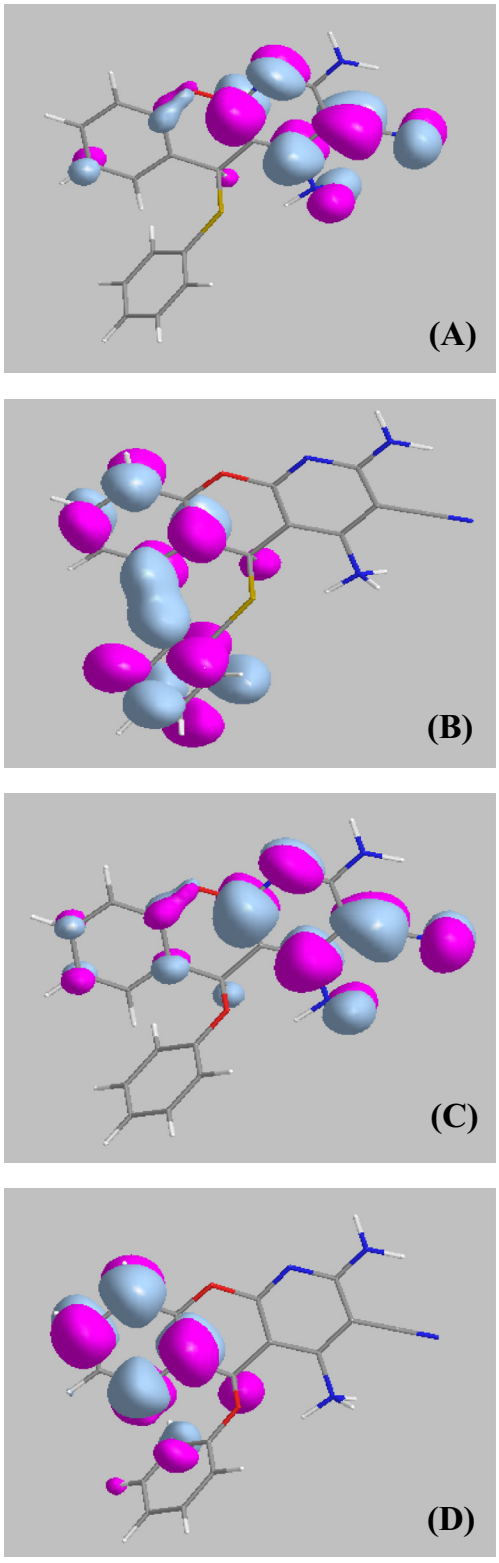

Figure 9 (a–d) Frontier molecular orbital's of protonated PPC-1 (a) HOMO, (b) LUMO and PPC-2 (c) HOMO, (d) LUMO.

Fig. 6(a) represents a highly corroded surface in the absence of inhibitors but as the PPCs are added the surface morphology becomes smooth (Fig. 6b and c), suggesting the formation of an inhibitor film over the N80 steel surface. The values of R_q and R_a in the absence of inhibitors are 75.54 μm and 56.73 μm. The values of R_q and R_a for PPC-1 are 1.84 μm and 1.69 μm, and for PPC-2 are 12.88 μm and 10.97 μm respectively. It could be observed that the values of R_q and R_a are large in the absence of PPCs, which is revealing a greater surface roughness. But in the presence of PPCs these values are reduced and this reduction in PPC-1 is larger than PPC-2, which confirms that the surface becomes smoother, and this smoothness occurs due to the formation of compact protective film of PPCs.

3.6. Quantum chemistry method

The optimized geometry, E_{HOMO} and E_{LUMO} of PPCs both in neutral and protonated forms are shown graphically in Figs. 7 (a–d), 8(a–d) and 9(a–d) respectively. As per the frontier molecular orbital theory, only frontier molecular orbital's i.e. HOMO and LUMO are only involved in the course of adsorption of the inhibitor molecules (Fang and Li, 2002). In general the higher the value of HOMO, higher would be the electron donating capacity of the inhibitor to vacant d-orbital of the metal. And lower the value of LUMO, greater would be the electron accepting ability of the inhibitor from the filled metal orbitals. But the most important parameter is ΔE, which is the energy difference between LUMO and HOMO. The lower the value of ΔE the easier would be the release of the electron and the stronger would the adsorption (Amin et al., 2010). It is said that to become a good corrosion inhibitor, it is not only the ability to donate the electron but also to accept it in the vacant orbitals (Zhang et al., 2010).

3.6.1. Neutral PPCs

The inspection of Table 3 reveals that the E_{HOMO} values of PPC-1 is greater than PPC-2, thus PPC-1 has more electron donating capacity than PPC-2. Also E_{LUMO} value of PPC-1 is lower than PPC-2, which makes PPC-1 to accept more electrons than PPC-2 from the filled d-orbital of N80 steel and causes its stronger adsorption. ΔE value of PPC-1 is lower than PPC-2, which causes PPC-1 to release the electron easily and in turn strengthen its adsorption. So, overall the adsorption order can be given as follows:

PPC-1 > PPC-2

3.6.2. Protonated PPCs

In aqueous media there is the possibility of the inhibitor to undergo protonation. These protonated PPCs then adsorb over the N80 steel surface. Thus the most negative site has been protonated and their molecular properties are reported in Table 3. Observing Table 3, we could say that ΔE values

Table 3 Calculated quantum chemical parameters of neutral PPCs.

Inhibitors	E_{HOMO} (eV)	E_{LUMO} (eV)	ΔE (eV)
PPC-1	−3.697	−1.242	2.455
PPC-2	−8.125	−0.783	7.342
PPC-1*	−1.592	−1.220	0.372
PPC-2*	−1.630	−0.764	0.866

* For protonated PPCs.

in protonated PPCs are less as compared to the neutral one, suggests that protonated PPCs have more reaction capacity than the neutral one. So, overall in the aqueous media protonated PPCs have more interaction ability than neutral ones.

4. Conclusion

EIS measurement showed the charge transfer process in PPCs. Tafel polarization reveals that both the inhibitors are cathodic. Both PPC-1 and PPC-2 obeyed the Langmuir adsorption isotherm. ΔG°_{ads} results showed the physical mode of adsorption for PPCs. Both in PPC-1 and PPC-2 the protonated molecule is dominating than the neutral molecule for adsorption.

Conflict of interest

The authors declare no competing financial interest.

Acknowledgement

K. R. Ansari gratefully acknowledges Ministry of Human Resource Development (MHRD), New Delhi, India for the financial assistance and facilitation of the study.

References

Ahamad, I., Prasad, R., Quraishi, M.A., 2010. Thermodynamic, electrochemical and quantum chemical investigation of some Schiff bases as corrosion inhibitors for mild steel in hydrochloric acid solutions. Corros. Sci. 52, 933–942.

Amin, M.A., Khaled, K.F., Mohsen, Q., Arida, H.A., 2010. A study of the inhibition of iron corrosion in HCl solutions by some amino acids. Corros. Sci. 52, 1684–1695.

Anejjar, A., Salghi, R., Zarrouk, A., Benali, O., Zarrok, H., Hammouti, B., Ebenso, E.E., 2014. Inhibition of carbon steel corrosion in 1 M HCl medium by potassium thiocyanate. J. Assoc. Arab Univ. Basic Appl. Sci. 15, 21–27.

Ansari, K.R., Quraishi, M.A., 2015a. Effect of three component (aniline–formaldehyde and piperazine) polymer on mild steel corrosion in hydrochloric acid medium. J. Assoc. Arab Univ. Basic Appl. Sci. 18, 12–18.

Ansari, K.R., Quraishi, M.A., 2015b. Experimental and computational studies of naphthyridine derivatives as corrosion inhibitor for N80 steel in 15% hydrochloric acid. Phys. E 69, 322–331.

Ansari, K.R., Yadav, D.K., Ebenso, E.E., Quraishi, M.A., 2012. Novel and effective pyridyl substituted 1,2,4-triazole as corrosion inhibitor for mild steel in acid solution. Int. J. Electrochem. Sci. 7, 4780–4799.

Ansari, K.R., Quraishi, M.A., Singh, A., 2014. Schiff's base of pyridyl substituted triazoles as new and effective corrosion inhibitors for mild steel in hydrochloric acid solution. Corros. Sci. 79, 5–15.

Ansari, K.R., Quraishi, M.A., Singh, A., 2015. Isatin derivatives as a non-toxic corrosion inhibitor for mild steel in 20% H_2SO_4. Corros. Sci. 95, 62–70.

Bammou, L., Belkhaouda, M., Salghi, R., Benali, O., Zarrouk, A., Zarrok, H., Hammouti, B., 2014. Corrosion inhibition of steel in sulfuric acidic solution by the *Chenopodium ambrosioides* extracts. J. Assoc. Arab Univ. Basic Appl. Sci. 16, 83–90.

Dahmani, M., El-Touhami, A., Al-Deyab, S.S., Hammouti, B., Bouyanzer, A., 2010. Corrosion inhibition of C38 steel in 1 M HCl: a comparative study of black pepper extract and its isolated piperine. Int. J. Electrochem. Sci. 5, 1060–1069.

Evdokimov, N.M., Kireev, A.S., Yakovenko, A.A., Antipin, M.Y., Magedov, I.V., Kornienko, A., 2007. One-step synthesis of heterocyclic privileged medicinal scaffolds by a multicomponent reaction of malononitrile with aldehydes and thiols. J. Org. Chem. 72, 3443–3453.

Fang, J., Li, J., 2002. Quantum chemistry study on the relationship between molecular structure and corrosion inhibition efficiency of amides. J. Mol. Struct. 593, 179–185.

Ferreira, E.S., Giancomelli, C., Giacomelli, F.C., Spinelli, A., 2004. Evaluation of the inhibitor effect of l-ascorbic acid on the corrosion of mild steel. Mater. Chem. Phys. 83, 129–134.

Frisch, M.J et al, 2007. Gaussian 03, Revision E.01. Gaussian Inc., Wallingford, CT.

Guan, N.M., Xueming, L., Fei, L., 2004. Synergistic inhibition between o-phenanthroline and chloride ion on cold rolled steel corrosion in phosphoric acid. Mater. Chem. Phys. 86, 59–68.

Karthikaiselvi, R., Subhashini, S., 2014. Study of adsorption properties and inhibition of mild steel corrosion in hydrochloric acid media by water soluble composite poly (vinyl alcohol-*o*-methoxy aniline). J. Assoc. Arab Univ. Basic Appl. Sci. 16, 74–82.

Mohamed, H.A., Rehim, M.H.A., 2015. Surface active hyperbranched polyamide–ester as a corrosion inhibitor for carbon steel in both neutral and acidic media. Anti-Corros. Methods Mater. 62, 95–102.

Musa, A.Y., Kadhum, A.A.H., Mohamad, A.B., Takriff, M.S., 2011. Molecular dynamics and quantum chemical calculation studies on 4,4-dimethyl-3-thiosemicarbazide as corrosion inhibitor in 2.5 M H_2SO_4. Mater. Chem. Phys. 129, 660–665.

Negm, N.A., Elkholy, Y.M., Tawfik, S.M., 2011. Corrosion inhibition of carbon steel by some quaternary surface active isoxazol-2-ium cationic Schiff bases in hydrochloric acid solution. Corros. Sci. 53, 3566–3575.

Obot, I.B., Obi-Egbedi, N.O., Odozi, N.W., 2010. Acenaphtho[1,2-b] quinoxaline as a novel corrosion inhibitor for mild steel in 0.5 M H_2SO_4. Corros. Sci. 52, 923–926.

Rosenfeld, I.L., 1981. Corrosion Inhibitors. McGraw-Hill, New York.

Shukla, S.K., Ebenso, E.E., 2011. Corrosion inhibition, adsorption behavior and thermodynamic properties of streptomycin on mild steel in hydrochloric acid medium. Int. J. Electrochem. Sci. 6, 3277–3291.

Solomon, M.M., Umoren, S.A., Udosoro, I.I., Udoh, A.P., 2010. Inhibitive and adsorption behaviour of carboxymethyl cellulose on mild steel corrosion in sulphuric acid solution. Corros. Sci. 52, 1317–1325.

Verma, C.B., Singh, P., Quraishi, M.A., 2016. A thermodynamical, electrochemical and surface investigation of Bis (indolyl) methanes as Green corrosion inhibitors for mild steel in 1 M hydrochloric acid solution. J. Assoc. Arab Univ. Basic Appl. Sci. 21, 24–30.

Xia, S., Qiu, M., Yu, L., Liu, F., Zhao, H., 2008. Molecular dynamics and density functional theory study on relationship between structure of imidazoline derivatives and inhibition performance. Corros. Sci. 50, 2021–2029.

Zhang, J., Liu, J., Yu, W., Yan, Y., You, L., Liu, L., 2010. Molecular modeling of the inhibition mechanism of 1-(2-aminoethyl)-2-alkyl-imidazoline. Corros. Sci. 52, 2059–2065.